

Active control of flow over a sphere for drag reduction at a subcritical Reynolds number

By SEJEONG JEON¹, JIN CHOI¹, WOO-PYUNG JEON¹,
HAECHON CHOI^{1†} AND JINIL PARK²

¹School of Mechanical and Aerospace Engineering, Seoul National University,
Seoul 151-744, Korea

²Division of Mechanical Engineering, Ajou University, Gyeonggi 443-749, Korea

(Received 30 December 2003 and in revised form 7 June 2004)

Active control of flow over a sphere at $Re = 10^5$, based on the free-stream velocity U_∞ and sphere diameter d , is carried out for drag reduction using a time-periodic blowing and suction from a slit on the sphere surface. The forcing frequency range considered is one to thirty times the natural vortex-shedding frequency. With the forcing, the drag on the sphere significantly decreases by nearly 50% for the forcing frequencies larger than a critical frequency (about $2.85U_\infty/d$). For the forcing frequencies smaller than this critical frequency, the drag is either nearly the same as, or slightly smaller than, that without forcing. The critical forcing frequency is found to be closely associated with the onset of the boundary-layer instability. It is shown from the surface-pressure measurement, surface oil-flow visualization and near-wall streamwise velocity measurement that the disturbances from the high-frequency forcing grow inside the boundary layer and delay the first separation while maintaining laminar separation, and they grow further along the separated shear layer and high momentum in the free stream is entrained toward the sphere surface, resulting in the reattachment of the flow (thus forming a separation bubble above the sphere surface) and the delay of the main separation. The reverse flow region in the wake is significantly reduced and the motion in that region also becomes weak owing to the forcing. Finally, the variation of drag by the present forcing with respect to the Reynolds number is very similar to that by dimples on the surface, but is different from that by surface roughness.

1. Introduction

Flow over a sphere is a typical bluff-body flow with many engineering applications. However, it has not been studied in depth as compared to flow over a circular cylinder because of the difficulties in the experimental set-up as well as in the computational approach for studying flow over a sphere. Nevertheless, there have been several studies on the characteristics of flow over a sphere (Fage 1936; Achenbach 1972; Achenbach 1974*a*; Taneda 1978; Kim & Durbin 1988; Sakamoto & Haniu 1990; Mittal 1999; Kim & Choi 2002; Yun, Choi & Kim 2003). Achenbach (1972) showed

† Author to whom correspondence should be addressed: choi@socrates.snu.ac.kr. Also at National CRI Center for Turbulence and Flow Control Research, Institute of Advanced Machinery and Design, Seoul National University, Korea.

the existence of four flow regions around the critical Reynolds number ($\approx 3.7 \times 10^5$) and explained their characteristics. In the subcritical region ($Re \leq 2 \times 10^5$), a laminar boundary-layer separation occurs around 80° from the stagnation point and the drag coefficient, C_d , is almost constant (≈ 0.5) irrespective of the Reynolds number. In the critical region ($2 \times 10^5 < Re \leq 3.7 \times 10^5$), C_d reduces rapidly to about 0.07 and a separation bubble(s) exists above the sphere surface. At Reynolds numbers larger than the critical Reynolds number, C_d increases slowly through the super- and trans-critical regions. Among these flow characteristics, the separation bubble observed near the critical region has received a special attention because it is closely associated with the so-called drag-crisis mechanism around the critical region (Fage 1936; Achenbach 1974*b*; Taneda 1978; Suryanarayana & Prabhu 2000). On the other hand, Kim & Durbin (1988) and Sakamoto & Haniu (1990) showed that there exist two distinct characteristic frequencies in flow over a sphere: one is the low frequency associated with the wake instability (vortex-shedding frequency) and the other is the high frequency related to the shear-layer instability.

Although several studies have been experimentally and numerically conducted for understanding the characteristics of flow over a sphere, there have been only a few works on control of flow over a sphere using passive and active devices (Achenbach 1974*b*; Bearman & Harvey 1976; Kim & Durbin 1988; Suryanarayana & Meier 1995; Suryanarayana & Prabhu 2000). As for passive devices, Achenbach (1974*b*) and Bearman & Harvey (1976) applied surface roughness and dimples on the sphere, respectively. Both studies achieved maximum drag reduction of nearly 50% in the sub-critical region, but the drag-reduction pattern by dimples was essentially different from that by surface roughness. That is, maximum drag reduction by dimples is maintained over a broad range of Reynolds numbers in the sub-critical region, whereas surface roughness produces maximum drag reduction only in a very narrow range of the Reynolds numbers. To the best of our knowledge, however, the detailed mechanism responsible for drag reduction by dimples or surface roughness has not been clearly presented yet, although it is believed to be associated with triggering the boundary-layer instability. This is mainly due to the measurement difficulty near the sphere surface. For example, the depth of dimples is comparable to the boundary-layer thickness and their shape is completely three-dimensional. Thus, even the wall pressure distribution itself is very hard to measure.

A different approach of controlling flow over a sphere was taken by Kim & Durbin (1988). Noting that there are two distinct frequencies existing in the shear layer and wake, they applied an acoustic forcing at a wide range of frequencies from the wake-instability frequency to the shear-layer-instability frequency to flow over a sphere at much lower Reynolds numbers ($Re \leq 10^4$) than those investigated using the passive control devices. They showed that the drag is increased significantly by the forcing and the size of the recirculation region is reduced with stronger motion inside, and they concluded that triggering the shear-layer instability or wake instability does not produce any drag reduction.

On the other hand, a popular active control device, called synthetic jet, has been used by many workers to manipulate many different flows. Among them, a recent work by Amitay, Smith & Glezer (1998) and Glezer & Amitay (2002) showed that the application of a high-frequency forcing from a synthetic jet to flow over a circular cylinder produces a significant drag reduction at sub-critical Reynolds numbers, and they attributed the mechanism to the 'virtual aero-shaping'. That is, the interaction of synthetic jets with an external cross-flow results in the formation of a separation bubble and thus apparent modification of the surface shape.

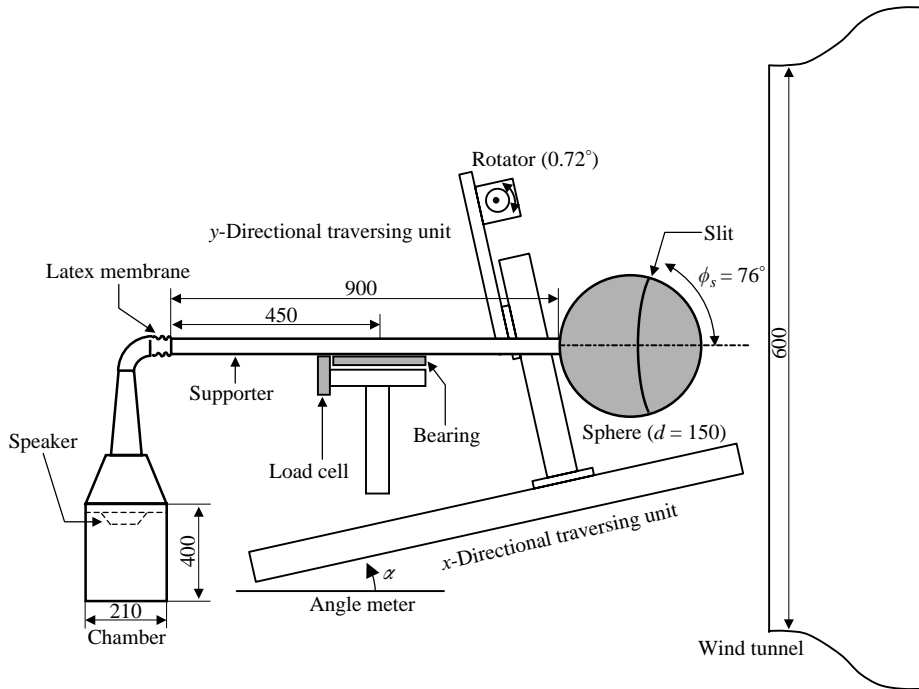


FIGURE 1. The experimental set-up (dimensions in mm).

In the present study, we perform an active control for drag reduction in flow over a sphere at sub-critical Reynolds numbers similar to those conducted for passive controls. We apply a time-periodic forcing (blowing and suction) at a wide range of forcing frequencies (covering the wake- and shear-layer-instability frequencies) from a slit located before the separation line. The main objective of the present study is to investigate how the low- to high-frequency forcing changes the boundary-layer characteristics before separation and how this change modifies the wake characteristics and the drag. Another objective is to see if the result obtained by Kim & Durbin (1988) is still valid at a sub-critical Reynolds number near $Re = 10^5$. The effect of the forcing on the drag and flow field near and behind the sphere is carefully investigated through the direct drag measurement, surface-pressure and velocity measurement, and flow visualization.

2. Experimental apparatus

Figure 1 shows the schematic diagram of the present experimental set-up, consisting of an open-type wind tunnel, sphere, supporter, speaker, load cell and traversing unit. The cross-section of the wind tunnel after contraction is $600 \text{ mm} \times 600 \text{ mm}$ and the turbulence intensity is lower than 0.5% at the free-stream velocity of 10 m s^{-1} . The sphere of 150 mm diameter is made of ABS resin. The Reynolds number for the present experiment is $Re = U_\infty d / \nu = 10^5$, where U_∞ is the free-stream velocity (10 m s^{-1}), d the sphere diameter, and ν the kinematic viscosity. An axisymmetric slit of 0.65 mm (about 0.5°) width is located on the sphere surface at the angle of $\phi_s = 76^\circ$ from the stagnation point (see figure 1), which is upstream of the separation line. A supporter (19 mm diameter pipe) attached to the sphere base is linked to a speaker chamber through a latex membrane.

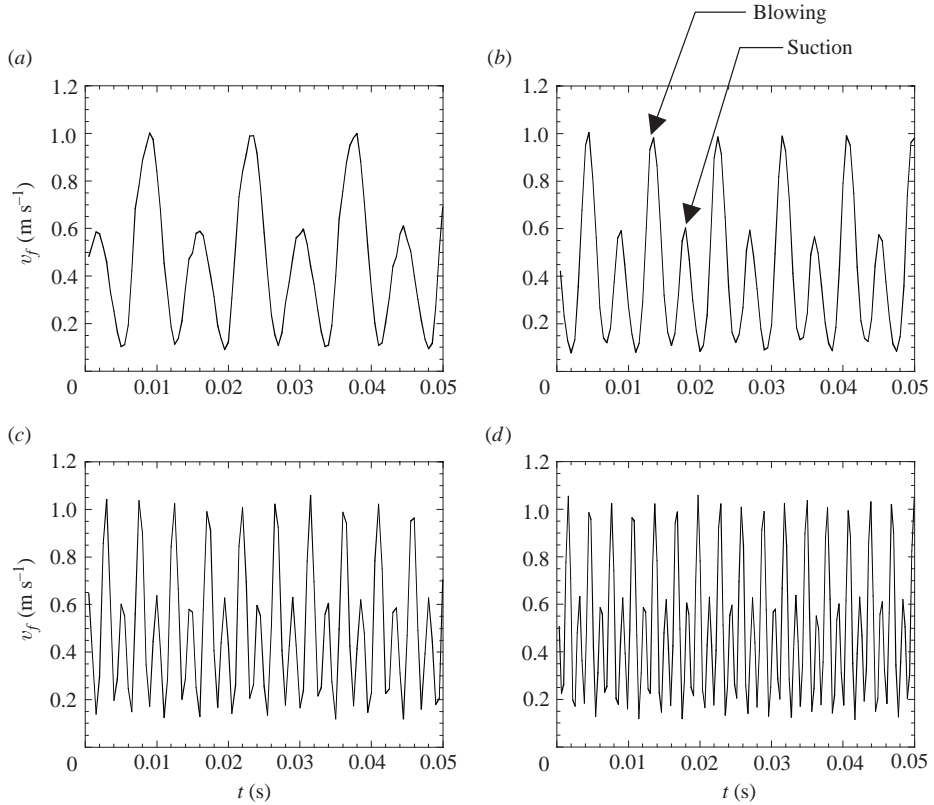


FIGURE 2. Temporal variations of the forcing velocity measured at the slit: (a) $St_d = 1.05$ ($f = 70$ Hz); (b) 1.65 (110 Hz); (c) 3.15 (210 Hz); (d) 4.95 (330 Hz).

The speaker generates a time-periodic blowing and suction of zero-net mass flux at a specified frequency from the slit. The forcing frequencies (f) applied are from 10 Hz to 370 Hz in increments of 20 Hz, corresponding to St_d ($= fd/U_\infty$) = 0.15 to 5.55 in increments of 0.3. For all the frequencies, the maximum velocity (or forcing amplitude) at the slit is tuned to be $v_{f,amp} = 0.5, 1$ and 1.5 m s $^{-1}$ (5, 10 and 15% of the free-stream velocity, respectively), by adjusting the voltage of the speaker. Figure 2 shows the temporal variations of the forcing velocity (v_f) measured at four different forcing frequencies using a single hot-wire probe in the case of $v_{f,amp} = 1$ m s $^{-1}$. The amplitude of blowing and suction is successfully kept at 10% of U_∞ as shown, even though low-frequency characteristics exist in v_f at a very high forcing frequency ($St_d = 4.95$). Note that the suction velocity is measured to be positive because the hot wire is insensitive to the flow direction. We verified the uniformity of the forcing along the slit by simultaneously measuring the forcing velocity at four different slit locations.

On the other hand, we attach a trip to the front surface of the sphere as a passive device for drag reduction by producing turbulent separation. The trip is composed of two wires of 0.5 mm diameter that locate at $\phi_s = 55^\circ$ and 60° on the sphere surface, respectively (a single wire of the same diameter is not sufficient to produce a turbulent boundary-layer flow before separation no matter where it is located). Then, we apply the present forcing with and without the trip, respectively, in order to observe different responses of the flow to forcing.

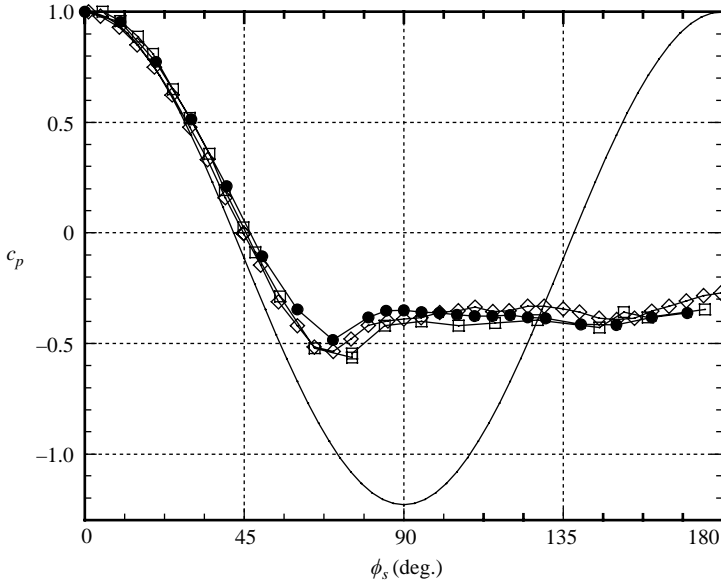


FIGURE 3. Static pressure distribution: ●, $Re = 10^5$ (present); □, $Re = 1.1 \times 10^5$ (Fage 1936); ◇, $Re = 1.62 \times 10^5$ (Achenbach 1972); —, potential flow.

The drag on the sphere is measured directly using a load cell (Cass BCL-1L). The magnitude of drag is small (0.25 ~ 0.50 N) and sensitive to the external interference, so that a careful measurement is required to minimize the measurement error. We repeat drag measurements at least ten times for each case and find that the uncertainty is $\pm 2.5\%$ (see error bars in figure 4). The surface pressure distribution in the azimuthal direction (ϕ_s) is measured through 23 taps with a scannivalve and a pressure transducer (MKS 220DD). The resolution of the pressure transducer is 0.001% at full scale of 10 Torr. The pressure distribution along the surface of the 'basic' sphere (i.e. without the trip and with the slit closed) is compared with those from the previous studies in figure 3, showing excellent agreement among the data. Also, the drag obtained from the integration of the surface pressure is almost the same as that by the load cell: the difference is within the uncertainty of direct drag measurement.

The velocity field is measured with an in-house multi-channel hot-wire anemometer and an I-type hot-wire probe. The hot-wire probe is positioned in the flow by a two-dimensional traversing unit (resolution is 0.02 mm) controlled automatically using a computer and a stepping motor. The sensor used is a platinum-10% rhodium wire of 2.5 μm diameter that is soldered to the prongs of the probe. At overheat ratio of 20%, the cutoff frequency of the sensor is approximately 25 kHz. The voltages from the anemometer are calibrated at the free stream with a standard two-hole Pitot tube and a digital manometer. A polynomial of fourth order is used to form a least-squares fit of the voltage versus the velocity. The uncertainty in measuring the velocity is $\pm 1\%$. Immediately after calibration, the probe is positioned in the flow and the data are recorded. After finishing measurements at each ϕ_s location, the probe is returned to the free stream and the calibration is checked. When the sensor drifts by more than 1%, the data are rejected and the calibration process is repeated. The output from the hot-wire sensor is sampled for 15 s at a rate of 16 kHz and is stored in a computer using an A/D converter (DT3016).

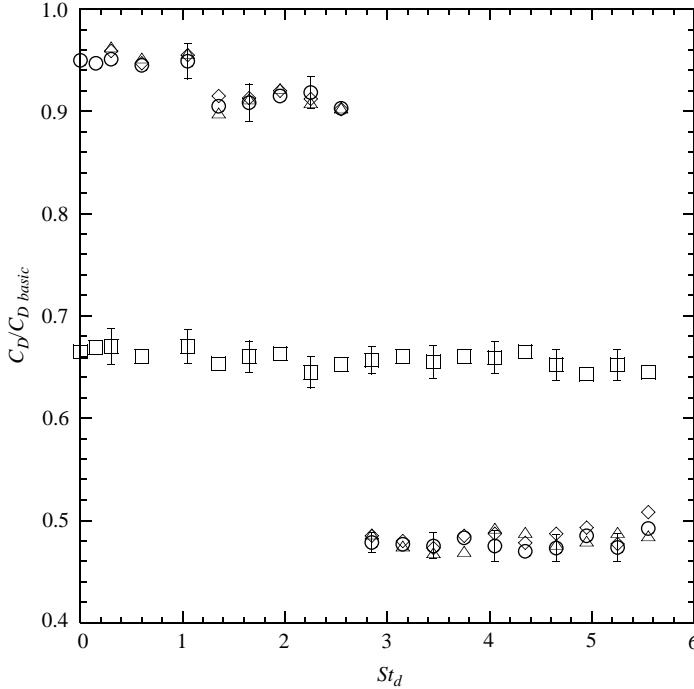


FIGURE 4. Variations of the drag coefficient with respect to the forcing frequency: \diamond , without trip, $v_{f,amp} = 0.05U_\infty$; \circ , without trip, $v_{f,amp} = 0.1U_\infty$; \triangle , without trip, $v_{f,amp} = 0.15U_\infty$; \square , with trip, $v_{f,amp} = 0.1U_\infty$. The vertical bars denote the measurement uncertainty obtained for $v_{f,amp} = 0.1U_\infty$.

3. Results and discussion

3.1. Drag variation

Figure 4 shows the variations of the drag coefficient with respect to the forcing frequency without and with the trip for three different forcing amplitudes of $v_{f,amp} = 0.05, 0.1$ and $0.15U_\infty$. Here, the drag coefficient is normalized by that of the basic sphere and $St_d = 0$ corresponds to the case of no forcing. Also shown in this figure is the uncertainty in measuring drag. The uncertainty is $\pm 2.5\%$ and is far smaller than the amount of drag reduction by the present forcing. The drag coefficient measured on the basic sphere ($C_{D basic}$) at $Re = 10^5$ is 0.51, which is in good agreement with the result of Achenbach (1972). It is shown in figure 4 that the drag variation is nearly insensitive to the forcing amplitude, at least in the range of $0.05 \leq v_{f,amp}/U_\infty \leq 0.15$ (the reason for this will be given in §3.3). In the following, therefore, the results obtained for $v_{f,amp} = 0.1U_\infty$ are discussed.

Without the trip, the drag at $St_d = 0$ decreases by about 5%, indicating that the flow is a little affected by the slit itself. With the forcing, the drag abruptly decreases by about 50% at a critical forcing frequency of $St_c (= f_c d/U_\infty) = 2.85$ and becomes nearly constant for $St_d > St_c$. For $St_d < St_c$, the drag is either nearly the same as, or slightly smaller than, that without forcing. On the other hand, the drag is reduced by 30% by the trip itself ($St_d = 0$), but the forcing does not reduce the drag further. Strikingly, the amount of drag reduction from the forcing in the absence of trip is larger than that from the forcing in the presence of trip. The reason for this will be explained in §3.2.

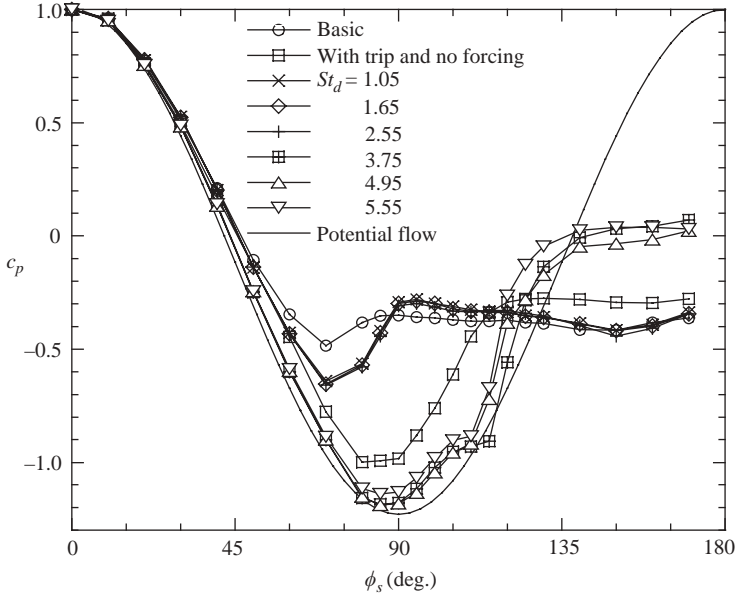


FIGURE 5. Static-pressure distribution on the sphere surface with the forcing frequency.

Figure 5 shows the surface-pressure distribution for different forcing frequencies in the absence of trip, together with those for the basic sphere, for the sphere in the presence of trip (slit closed, with trip and no forcing) and for the potential flow. The form drag exerted on the sphere is determined by integrating the pressure coefficient along the azimuthal angle:

$$C_{D_p} = \int_0^\pi c_p \sin 2\phi_s d\phi_s. \quad (1)$$

For $St_d < St_c = 2.85$, the pressure distributions are similar to that on the basic sphere except near $\phi_s = 70^\circ$ where the contribution to the drag is small, indicating negligible or small drag reduction at these forcing frequencies. On the other hand, for $St_d > St_c$, the surface pressures at $\phi_s < 135^\circ$ are nearly the same as or similar to the inviscid pressure and the pressures at $\phi_s \geq 135^\circ$ are much larger than those on the basic sphere, indicating that a significant amount of drag reduction should occur at these high forcing frequencies. The pressure on the tripped sphere is close to that of the high-frequency forcing at $\phi_s < 90^\circ$, but becomes close to that on the basic sphere at $\phi_s > 120^\circ$, confirming less drag reduction by the trip than by the forcing at $St_d > St_c$.

It should be mentioned here that there exists a plateau in the pressure curve around $\phi_s = 110^\circ$ for the high-frequency forcing cases ($St_d > 2.85$). As shown in figure 6, this pressure pattern is very similar to that observed in the unforced flow at the critical Reynolds number where the drag coefficient decreases very rapidly and a separation bubble exists above the sphere surface (Fage 1936; Achenbach 1974*b*; Taneda 1978; Suryanarayana & Meier 1995), suggesting an important clue to the present drag-reduction mechanism by the present high-frequency forcing. Also, we observed an asymmetric distribution of the surface pressures measured at four different spanwise angles for the high-frequency forcing case. The flow asymmetry was also found by Taneda (1978) and Suryanarayana & Prabhu (2000) at the critical Reynolds number where the separation bubble was observed.

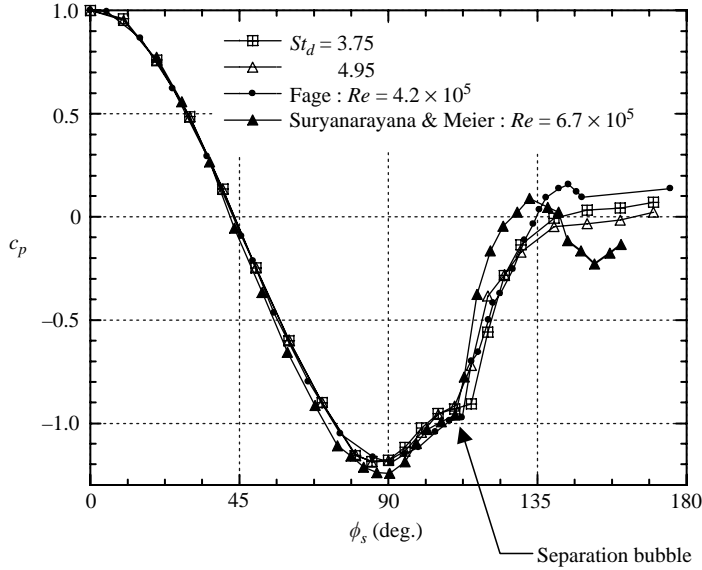


FIGURE 6. Static-pressure distributions on the controlled sphere at $Re = 10^5$ (present study) and on the basic sphere in the critical region (Fage 1936; Suryanarayana & Meier 1995).

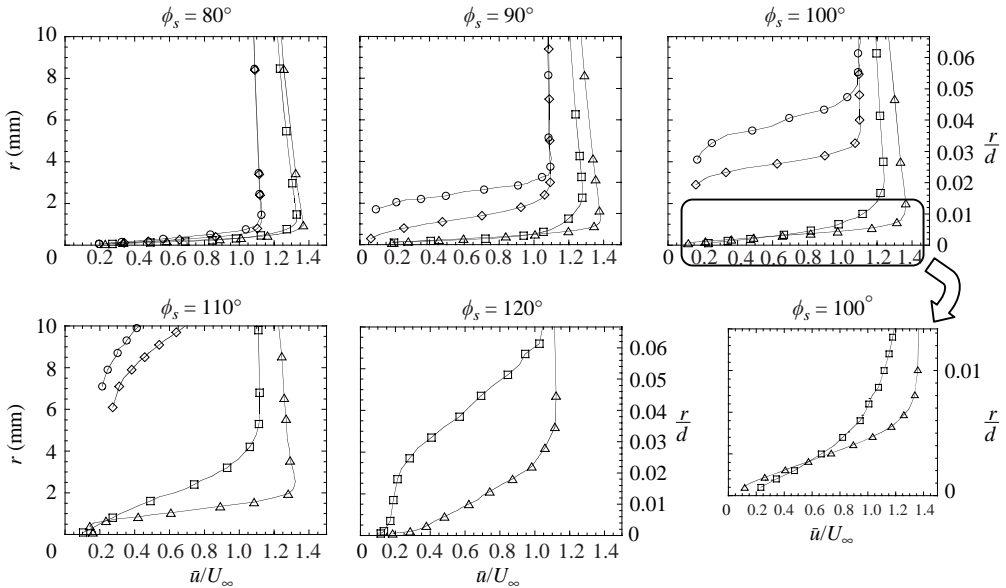


FIGURE 7. Profiles of the mean streamwise velocity (\bar{u}) above the sphere surface at $\phi_s = 80^\circ \sim 120^\circ$: \circ , basic; \square , with trip and no forcing; \diamond , $St_d = 1.65$; \triangle , $St_d = 4.95$. Here, r denotes the wall-normal distance from the surface.

3.2. Velocity measurement and visualization

Figure 7 shows the profiles of the mean streamwise velocity measured with a hot-wire probe along the radial direction from the sphere surface at $\phi_s = 80^\circ \sim 120^\circ$. For the case of the basic sphere, a thin boundary-layer flow is formed at $\phi_s = 80^\circ$, but the flow is detached from the wall at $\phi_s = 90^\circ$, showing that separation occurs between

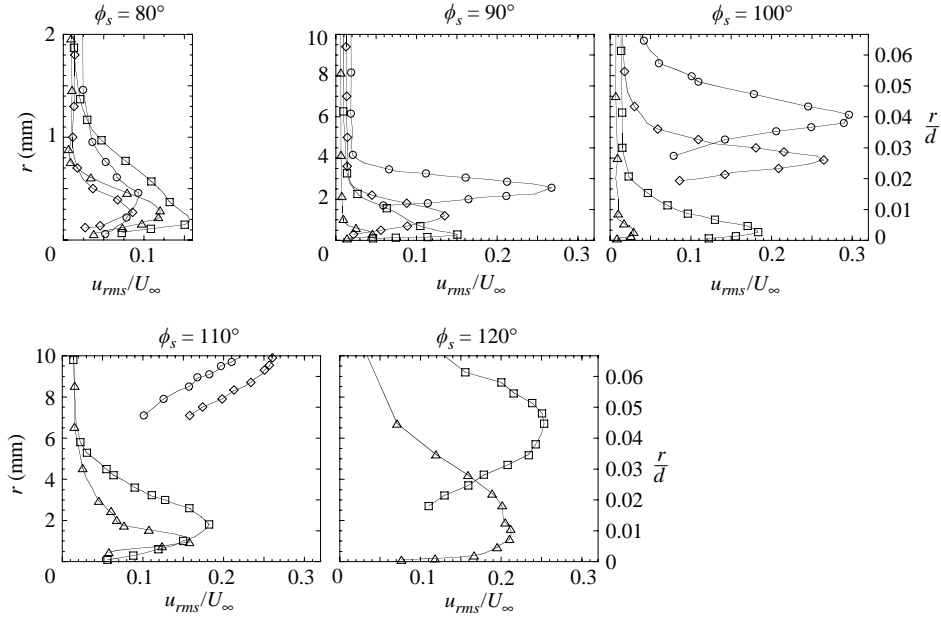


FIGURE 8. Profiles of the r.m.s. streamwise velocity fluctuations (u_{rms}) above the sphere surface at $\phi_s = 80^\circ \sim 120^\circ$: \circ , basic; \square , with trip and no forcing; \diamond , $St_d = 1.65$; \triangle , $St_d = 4.95$.

$\phi_s = 80^\circ$ and 90° . In the case of low-frequency forcing ($St_d = 1.65$), the near-wall velocity gradient at $\phi_s = 80^\circ$ is a little larger and the shear-layer thickness after separation (at 90° and 100°) is smaller than those in the case of the basic sphere, implying that separation is slightly delayed owing to the low-frequency forcing.

On the other hand, the flow above the tripped sphere at $\phi_s = 80^\circ \sim 100^\circ$ represents the characteristics of a turbulent boundary-layer, i.e. a thick boundary-layer flow, a fuller mean velocity profile near the wall, broad-band energy spectrum (see below), etc. The boundary layer begins to separate from the surface at $\phi_s = 110^\circ$ and separates completely at $\phi_s = 120^\circ$. In case of the high-frequency forcing ($St_d = 4.95$), the flow maintains laminar boundary-layer characteristics up to $\phi_s = 100^\circ$, i.e. a thin boundary layer and non broadband energy spectrum (see below).

Note that the momentum of the flow very near the wall is still larger in case of the tripped sphere than in the case of high-frequency forcing (see the velocity profiles at $\phi_s = 100^\circ$ in figure 7), even though the mean velocity away from the wall is more accelerated in the latter case. Because of this lower mean velocity gradient very near the wall, the boundary layer in the case of high-frequency forcing separates from the wall earlier than in the case of the tripped sphere; the boundary layer separates at $\phi_s = 110^\circ$ in the case of high-frequency forcing, as shown in figure 7. However, the separation region is limited very near the wall because the flow has a high momentum outside, as mentioned above. Therefore, at $\phi_s = 120^\circ$, the flow with high-frequency forcing has already reattached to the wall, indicating that a separation bubble exists at $100^\circ < \phi_s < 120^\circ$ owing to the forcing.

Figure 8 shows the profiles of the root-mean-square (r.m.s.) streamwise velocity fluctuations in the radial direction at $\phi_s = 80^\circ \sim 120^\circ$. In the cases of the basic sphere and the low-frequency forcing, u_{rms} increases very rapidly in the shear layer after separation, whereas the profile of u_{rms} in the presence of trip develops to that of the characteristic turbulent boundary-layer flow before separation at $\phi_s = 110^\circ$. In the case

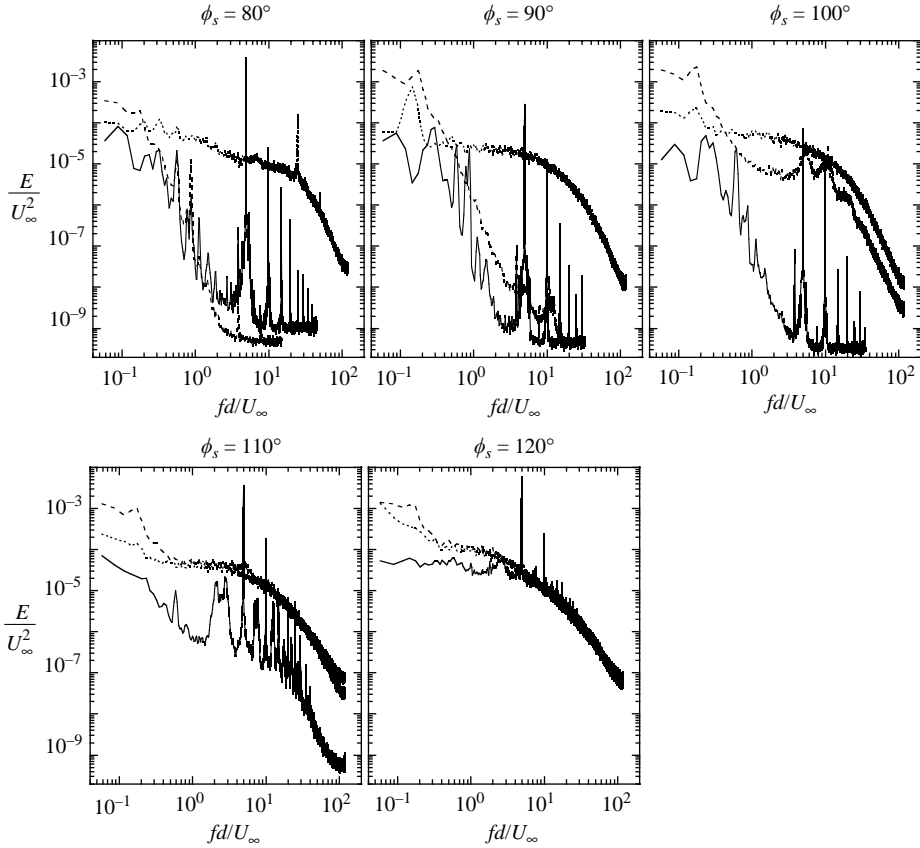


FIGURE 9. Energy spectra of the streamwise velocity at the radial location of having maximum u_{rms} : — —, basic; ···, with trip and no forcing; —, $St_d = 4.95$.

of the high-frequency forcing, u_{rms} slowly decreases before separation, i.e. at $\phi_s \leq 100^\circ$, owing to the mean velocity acceleration there. After first separation ($\phi_s = 110^\circ$), u_{rms} increases very rapidly along the separated shear layer, and turbulent-boundary-layer characteristics develop near the wall after reattachment ($\phi_s = 120^\circ$).

At each ϕ_s , the streamwise velocity signal at the radial location where u_{rms} is maximum is Fourier-transformed to obtain its energy spectrum. Therefore, before separation, the spectra are obtained inside the boundary layer for all the cases investigated, whereas they are obtained in the separating shear layer after separation. Figure 9 shows the energy spectra of the streamwise velocity at $\phi_s = 80^\circ \sim 120^\circ$ for the cases of the basic and tripped spheres and for the high-frequency forcing case. For the basic sphere, the energy spectra at $\phi_s = 80^\circ \sim 100^\circ$ show the characteristics of laminar and transitional flows, and a distinct peak at $fd/U_\infty = 0.18$ observed for $\phi_s \geq 90^\circ$ clearly indicates the vortex-shedding frequency, which agrees well with the results of previous studies (Achenbach 1974a; Kim & Durbin 1988). In the presence of the trip, the spectra show the characteristics of turbulent boundary-layer flow at $\phi_s \geq 80^\circ$, indicating that the boundary-layer flow before separation is fully turbulent. Therefore, the addition of time-periodic forcing into the boundary layer in the presence of the trip does not contribute to further drag reduction (figure 4) because the boundary layer is already turbulent there. For the high-frequency forcing,

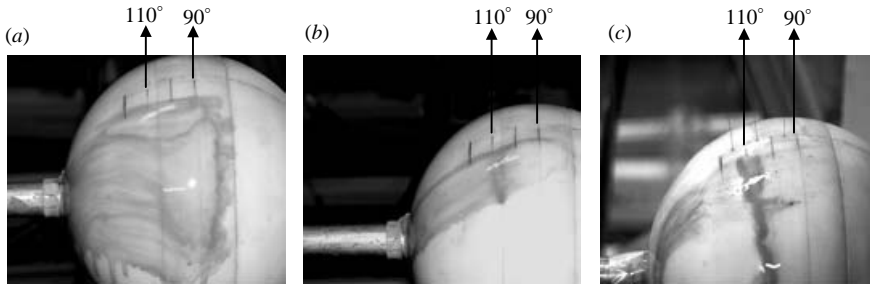


FIGURE 10. Oil flow pattern on the sphere surface: (a) basic; (b) with trip and no forcing; (c) $St_d = 4.95$. Here, the flow is from right to left.

the peaks are found at the forcing frequency and its harmonic frequencies. The boundary-layer flow is more likely to be laminar before separation, but the energy at intermediate and high frequencies increases very rapidly at $\phi_s = 110^\circ$ (after separation) and the spectrum becomes broadband at 120° (after reattachment), which indicates that fluctuations rapidly increase at all scales along the separated shear layer, resulting in the reattachment of the flow on the sphere surface.

Achenbach (1974*b*) indicated that the low drag coefficient at the critical Reynolds numbers is due to the existence of a separation bubble above the sphere surface. That is, with a separation bubble, the reattached flow has high momentum near the wall with large turbulence intensity, which delays the main separation. The phenomenon observed at the critical Reynolds number is very similar to the present one with high-frequency forcing, suggesting that large drag reduction achieved for $St_d > St_c$ is essentially associated with the generation of the separation bubble above the sphere surface.

Figure 10 shows the surface oil flow pattern visualized by coloured oil paint. In the case of the basic sphere, separation occurs between 80° and 90° , whereas in the presence of the trip, separation is delayed and occurs at $\phi_s = 105^\circ \sim 110^\circ$. In the case of $St_d = 4.95$, separation is delayed and occurs at $\phi_s = 105^\circ \sim 110^\circ$, and then the flow reattaches to the surface at $\phi_s = 110^\circ \sim 115^\circ$, forming a separation bubble there. The main separation occurs at $\phi_s \simeq 130^\circ$. The flow pattern observed here is consistent with the hot-wire measurement shown in figure 7.

Figure 11 shows the flow visualization using smoke wires located in front of and immediately after the sphere. Again, it is clear that, with the high-frequency forcing, the detaching shear layer is attracted to the sphere surface and the size of the recirculation region is reduced as compared to the cases of the basic and tripped spheres. We have tried to visualize the separation bubble generated at $\phi_s \approx 110^\circ$ in the case of high-frequency forcing, but failed because of its small size. The separation bubble produced by the high-frequency forcing does not seem to be transitory, but to be stationary. This conjecture arises because the flow patterns observed by several attempts of smoke-wire visualization have been nearly the same as that shown in figure 11(c); also, the real-time hot-wire signal inside the separation bubble is quiet regardless of the forcing frequency.

3.3. Critical forcing frequency

So far, we have shown that the drag on the sphere was reduced by 50% when the forcing frequency was larger than the critical frequency of $St_c = 2.85$. This high-frequency forcing generated a small separation bubble above the sphere surface

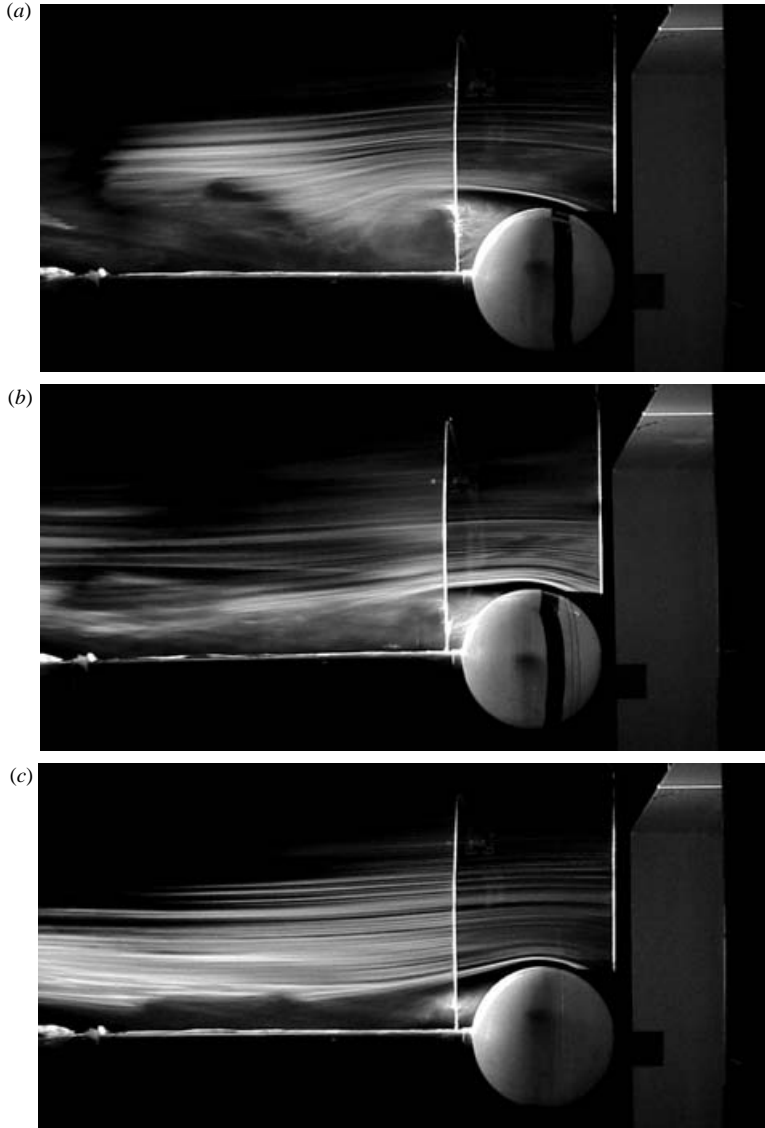


FIGURE 11. Smoke flow visualization: (a) basic; (b) with trip and no forcing; (c) $St_d = 4.95$. Here, the flow is from right to left.

at around 110° from the stagnation point and delayed the main separation. The critical forcing frequency ($St_c = 2.85$) obtained in the present study is very different from the frequencies corresponding to the wake instability ($St_d = 0.18$) and shear-layer instability ($St_d \approx 10$ from Kim & Durbin 1988). Therefore, the critical forcing frequency should be related to the boundary-layer instability as shown below. Because the momentum thickness before separation is very thin as compared to the sphere diameter (i.e. $\theta/d < 1/1000$) and also the instability in a boundary layer containing two-dimensional curvature (like the boundary layer above the sphere) has not been studied yet, we simply resort to a boundary-layer flow of the Falkner–Skan class

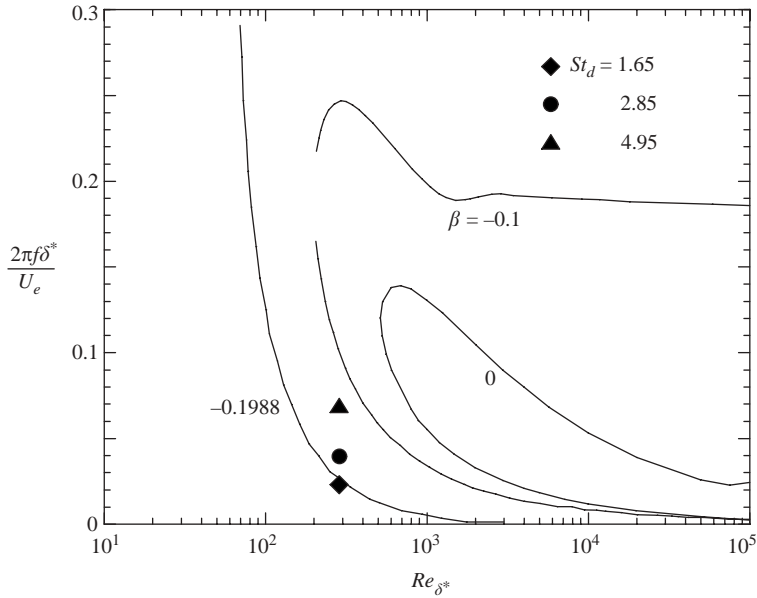


FIGURE 12. Neutral stability curves for the Falkner–Skan class flows (Morgan *et al.* 1999).

accepting some possible detailed differences in the instability characteristics between two flows.

Figure 12 shows the neutral stability curves obtained from the linear stability theory for the Falkner–Skan class flows by Morgan, Rubin & Khosla (1999). The abscissa in this figure is the Reynolds number based on the displacement thickness and the ordinate is the non-dimensional frequency of small perturbation. Here, δ^* is the displacement thickness, f is the frequency, $\beta (= 2m/(m+1))$ is the non-dimensional pressure gradient, m is an exponential parameter in Falkner–Skan equations (i.e. $U(x) = Cx^m$). $\beta = 0$ corresponds to zero pressure gradient and $\beta = -0.1988$ to the adverse pressure gradient at separation. We measured both δ^* and β from the mean streamwise velocity profile in the radial direction and the wall-pressure gradient at $\phi_s = 80^\circ$ (a location immediately before separation), resulting in $\beta \approx -0.15$ and $Re_{\delta^*} \approx 285$. Also, our forcing frequencies of $St_d = 1.65, 2.85$ and 4.95 are converted to be $2\pi f \delta^*/U_e = 0.023, 0.04$ and 0.07 , plotted with closed symbols in figure 12, where U_e is the boundary-layer edge velocity. It is clear in this figure that the forcing frequency of $St_d = 4.95$ is within the unstable region, but the forcing frequency of $St_d = 1.65$ is not. Therefore, we may conclude that the critical forcing frequency of $St_c = 2.85$ is directly associated with the boundary-layer instability.

Note, however, that the linear instability analysis by Morgan *et al.* (1999) is only valid for small-disturbance amplitudes, but the present forcing amplitudes are relatively large. Therefore, we apply three different forcing amplitudes of $v_{f,amp} = 0.05, 0.1$ and $0.15U_\infty$ at two different forcing frequencies of $St_d = 1.65$ and 3.90 and measure the growth of the energy at the forcing frequency in a short streamwise distance, for the validity of the argument based on the linear stability. Figure 13 shows the evolution of energy in the streamwise velocity fluctuations at the forcing frequency ($St_d = 1.65$ or 3.90) along the streamwise direction for the three forcing amplitudes, where the energy is obtained at the radial location of maximum u_{rms} for each ϕ_s . As shown, the growth of energy in the streamwise direction is

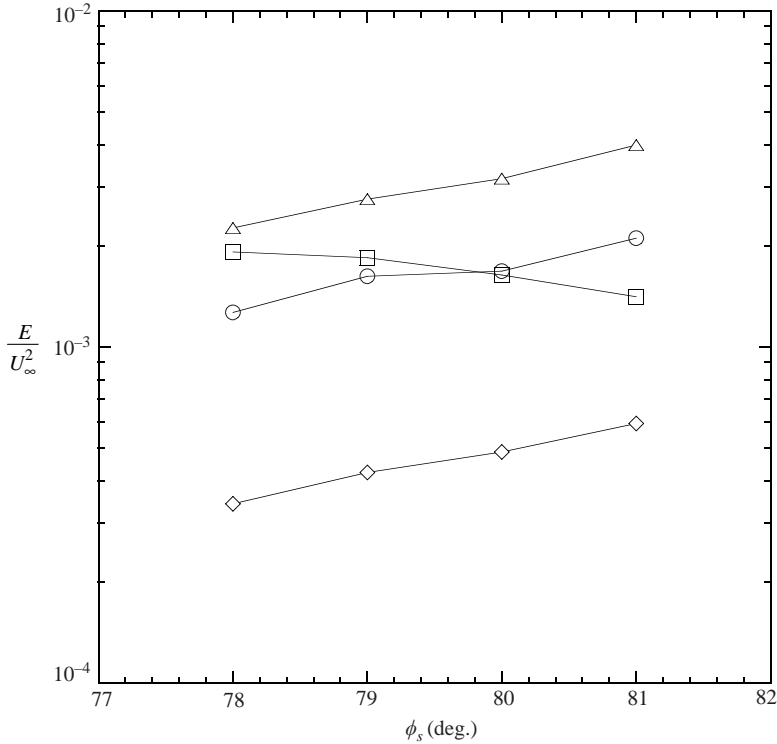


FIGURE 13. Evolution of energy in the streamwise velocity fluctuations at the forcing frequency along the streamwise direction for three different forcing amplitudes: \diamond , $v_{f,amp} = 0.05U_\infty$ and $St_d = 3.90$; \circ , $v_{f,amp} = 0.1U_\infty$ and $St_d = 3.90$; \triangle , $v_{f,amp} = 0.15U_\infty$ and $St_d = 3.90$; \square , $v_{f,amp} = 0.15U_\infty$ and $St_d = 1.65$.

manifest and the growth rates for three forcing amplitudes are nearly the same in the case of high-frequency forcing ($St_d = 3.90$), but the energy decays for $St_d = 1.65$, which clearly supports the use of linear instability argument for the existence of the critical forcing frequency.

It is worth mentioning the study of Kim & Durbin (1988), who applied an acoustic forcing at various forcing frequencies from the wake-instability frequency to the shear-layer-instability frequency to the flow over a sphere at $Re \leq 10^4$. They found that the drag increased for all the forcing frequencies at those Reynolds numbers. When we convert those Reynolds numbers to Re_{δ^*} , they are much smaller than $Re_{\delta^*} = 100$. At this Reynolds number range (see figure 12), acoustic perturbations could not trigger the boundary-layer instability, but trigger the wake instability or the shear-layer instability, resulting in drag increase. Their result is another indication that the present high-frequency forcing triggers the boundary-layer instability.

Amitay *et al.* (1998) and Glezer & Amitay (2002) showed that the application of a high-frequency forcing ($St_d = 6.1$, 2.6 and 1.5, respectively, for $Re = 31\,000$, 75 000 and 131 000) from a synthetic jet to flow over a circular cylinder produced a significant drag reduction, although the lift was increased by the forcing because the actuator was installed at only one side of the cylinder. They also applied two different forcing frequencies of $St_d = 2.6$ and 4.5 for $Re = 75\,000$ and found that the drag variation was insensitive to the forcing frequency. These results are similar to what we observed from

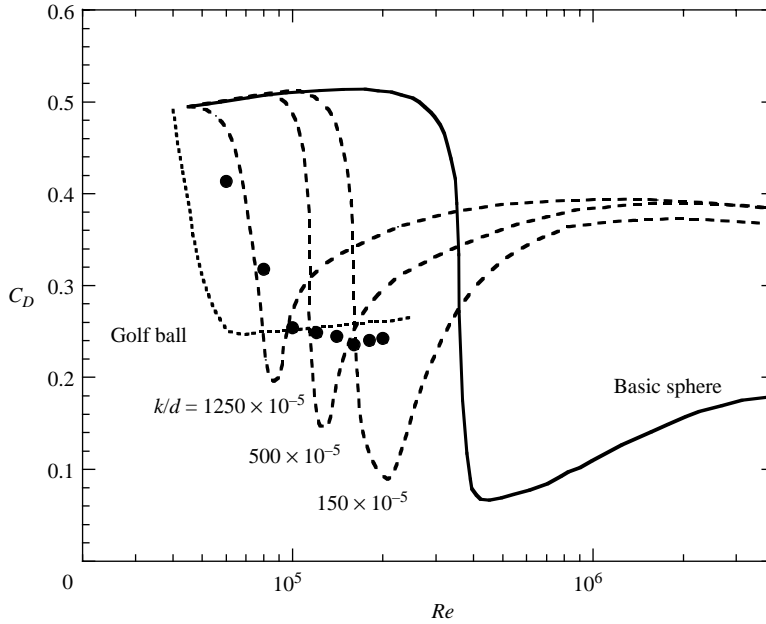


FIGURE 14. Variations of the drag coefficient owing to active and passive controls as a function of the Reynolds number: \bullet , present study; \cdots , dimples (golf ball) by Bearman & Harvey (1976); $---$, roughness (k/d) by Achenbach (1974b).

the high-frequency forcing in the present study. Amitay *et al.* (1998) and Glezer & Amitay (2002) explained the mechanism of drag reduction in terms of ‘virtual aeroshaping.’ That is, their high-frequency forcing induces a local separation bubble above the cylinder surface, which acts as a ‘virtual surface’ and displaces local streamlines well outside the undisturbed boundary layer, resulting in rapid decrease in the surface pressure both upstream and downstream of the forcing location because the potential flow outside the surface boundary-layer moves faster than the unforced flow. In this section, however, we suggested a different drag-reduction mechanism based on the boundary-layer instability.

3.4. Effect of the Reynolds number

Figure 14 shows the variations of the drag coefficient owing to active and passive controls as a function of the Reynolds number. It is shown in Achenbach (1974b) that, with surface roughness, the drag coefficient decreases sharply and then increases rapidly with increasing Reynolds number, showing a local minimum at a critical Reynolds number (Re_c). This critical Reynolds number decreases with increasing roughness. Also, the drag coefficient at $Re > Re_c$ increases more sharply at larger roughness and approaches 0.4. On the other hand, dimples reduce the drag coefficient, even at a lower Reynolds number than surface roughness does (Bearman & Harvey 1976). After its decrease by dimples, the drag coefficient remains almost constant at about 0.25.

In the present study, we change the Reynolds number by changing the free-stream velocity ($U_\infty = 6 \text{ m s}^{-1} \sim 20 \text{ m s}^{-1}$). We fix the forcing frequency to be $f = 330 \text{ Hz}$ ($fd/U_\infty = 4.95$ at $Re = 10^5$) and the amplitude of the blowing and suction to be 1 m s^{-1} for different Reynolds numbers, because the result is nearly insensitive to the amplitude and frequency of the forcing once $St_d > St_c$ (figure 4). The result of the

present high-frequency forcing is similar to that by dimples. That is, after its rapid decrease due to the present forcing, the drag coefficient remains almost constant at about 0.24. The present result suggests that the mechanism of drag reduction by dimples may be similar to that by the present high-frequency forcing, i.e. the generation of a separation bubble, reattachment of the flow and delay of main separation, although the detailed cause of such changes may not be the same (note that dimples generate essentially three-dimensional disturbances to the flow).

4. Concluding remarks

In the present study, an active control of flow over a sphere was conducted for drag reduction using a time-periodic blowing and suction at a sub-critical Reynolds number of $Re = 10^5$. The forcing-frequency range considered was one to thirty times the natural vortex-shedding frequency. With the periodic blowing and suction, the drag on the sphere decreased by nearly 50% for forcing frequencies larger than a critical frequency (about $2.85U_\infty/d$). For forcing frequencies smaller than this critical frequency, drag was either nearly the same as, or slightly smaller than, that without forcing.

It was shown from the surface-pressure measurement, visualization and near-wall velocity measurement that the present high-frequency forcing generates a separation bubble above the sphere surface and delays the main separation, resulting in a large drag reduction. That is, at a forcing frequency larger than the critical frequency, the disturbances grew inside the boundary layer and delayed the first separation from $\phi_s = 82^\circ$ to about 105° while maintaining laminar separation. They grew further along the separated shear layer and high momentum in the free stream was entrained toward the sphere surface, resulting in the reattachment of the flow (thus forming a separation bubble above the sphere surface) and the delay of the main separation. On the other hand, at a low frequency forcing, the disturbances decayed along the streamwise direction inside the boundary layer. The existence of the critical forcing frequency was supported by the boundary-layer instability analysis. The reattachment of the flow on the sphere surface was associated with the instability of the separated shear layer, where the strong incoming disturbances triggering the shear-layer instability came from the boundary-layer instability.

We believe that the generation of the separation bubble above the sphere surface is important in obtaining a large amount of drag reduction, which has also been observed in the unforced flow at the critical Reynolds number where the drag crisis occurs. Our belief comes from the fact that reaching a turbulent boundary-layer flow before separation by the trip produces less drag reduction than that by high-frequency forcing. Therefore, the present forcing strategy should also work for drag reduction in flow over a circular cylinder at a high Reynolds number in the sub-critical region. It was also shown in this paper that the variation of drag reduction by the present forcing with respect to the Reynolds number is very similar to that by dimples, suggesting that the mechanism of drag reduction by dimples may be similar to that by the present forcing.

In our study, we have shown that the initial disturbances from the present two-dimensional high-frequency forcing grow owing to the boundary-layer instability and they rapidly grow along the separated shear layer, resulting in the reattachment of the flow and the delay of the main separation. However, it is known that the separated shear layer is unstable to three-dimensional disturbances, and also the boundary layer is receptive to three-dimensional disturbances when the initial disturbance amplitude

is large enough. Therefore, it would be interesting to know whether or not three-dimensional disturbances are more effective in reducing drag for flow over a sphere than the present two-dimensional disturbances. As shown in this study, however, reaching turbulent boundary layer before separation by the trip did not produce as much drag reduction as that by the present two-dimensional high-frequency forcing. Hence, an intensive study is required to draw a firm conclusion about the effectiveness of three-dimensional disturbances as compared to two-dimensional disturbances, which is an important study to be carried out in the near future.

This work was supported by the Creative Research Initiatives of the Korean Ministry of Science and Technology.

REFERENCES

- ACHENBACH, E. 1972 Experiments on the flow past spheres at very high Reynolds numbers. *J. Fluid Mech.* **54**, 565–575.
- ACHENBACH, E. 1974a Vortex shedding from sphere. *J. Fluid Mech.* **62**, 209–221.
- ACHENBACH, E. 1974b The effect of surface roughness and tunnel blockage on the flow past spheres. *J. Fluid Mech.* **65**, 113–125.
- AMITAY, M., SMITH, B. L. & GLEZER, A. 1998 Aerodynamic flow control using synthetic jet technology. *AIAA Paper* 98-0208.
- BEARMAN, P. W. & HARVEY, J. K. 1976 Golf ball aerodynamics. *Aeronaut. Q.* May, 112–122.
- FAGE, A. 1936 Experiments on a sphere at critical Reynolds numbers. *Aero. Res. Council. R & M* 1766.
- GLEZER, A. & AMITAY, M. 2002 Synthetic jets. *Annu. Rev. Fluid Mech.* **34**, 503–529.
- KIM, D. & CHOI, H. 2002 Laminar flow past a sphere rotating in the streamwise direction. *J. Fluid Mech.* **461**, 365–386.
- KIM, H. J. & DURBIN, P. A. 1988 Observations of the frequencies in a sphere wake and of drag increase by acoustic excitation. *Phys. Fluids* **31**, 3260–3265.
- MITTAL, R. 1999 Planar symmetry in the unsteady wake of a sphere. *AIAA J.* **37**, 388–390.
- MORGAN, P. E., RUBIN, S. G. & KHOSLA, P. K. 1999 Application of the reduced Navier–Stokes methodology to flow stability of Falkner–Skan class flows. *Comput. Fluids* **28**, 307–327.
- SAKAMOTO, H. & HANIU, H. 1990 A study on vortex shedding from spheres in a uniform flow. *Trans. ASME I: J. Fluids Engng* **112**, 386–392.
- SURYANARAYANA, G. K. & MEIER, G. E. A. 1995 Effect of ventilation on the flow field around a sphere. *Exps. Fluids* **19**, 78–88.
- SURYANARAYANA, G. K. & PRABHU, A. 2000 Effect of natural ventilation on the boundary-layer separation and near-wake vortex shedding characteristics of a sphere. *Exps. Fluids* **29**, 582–591.
- TANEDA, S. 1978 Visual observations of the flow past a sphere at Reynolds number between 10^4 and 10^6 . *J. Fluid Mech.* **85**, 187–192.
- YUN, G., CHOI, H. & KIM, D. 2003 Turbulent flow past a sphere at $Re = 3700$ and 10^4 . *Phys. Fluids* **15**, S6.